Morphology and Seebeck Coefficients of Electrodeposited Bi₂Se₃ Films Grown onto Au(111)/Si Substrates

Rasin Ahmed, a,† Md Golam Rosul, a,† Yin Xu, Mona Zebarjadia,b and Giovanni Zangarib,*

^aDepartment of Electrical and Computer Engineering, University of Virginia, Charlottesville, VA 22904

^bDepartment of Materials Science and Engineering, University of Virginia, Charlottesville, VA 22904

Abstract

Polymorphism in Bi₂Se₃ allows it to be tuned for unique electrical, thermal, and optical properties. The commonly reported rhombohedral structure is a topological insulator, a narrow gap semiconductor with a bandgap of 0.2 - 0.3 eV, and has been widely studied for thermoelectric applications. The alternative orthorhombic structure is a semiconductor with a larger bandgap of 0.9 - 1.2 eV. The opportunity to fabricate a mixture of these orthorhombic and rhombohedral structures provides a chance for materials engineering to optimize its electrical and thermal properties. Here we report the morphology and the Seebeck coefficient of mixed-phase, Se-rich, n-type Bi₂Se₃ films prepared by electrodeposition using an acidic bath. Post-nucleation formation of smooth films was observed to be followed by the emergence of crystals and continued growth through the coalescence of the newly formed crystals. The room temperature Seebeck coefficients of the films were also observed to vary as a function of the film thickness, increasing from -90 µV/K (0.74 µm thickness) to a maximum of -184.4 µV/K (1.84 µm thickness) and gradually decreasing to -100.8 µV/K (5.72 µm thickness). Analysis of XRD patterns for the Bi₂Se₃ films showed that the thickness dependence of Seebeck coefficients was related to the transition from pure rhombohedral to a mixture of orthorhombic and rhombohedral phases. The thickness dependent Seebeck effect was further discussed by the computational study of the Bi₂Se₃ band structures and Seebeck coefficients of pure rhombohedral and pure orthorhombic structures.

1. Introduction

V-VI chalcogenide compounds such as Bi_2Ch_3 (Ch = S, Se, or Te) and the homologous series based on Sb, exhibit a wide range of properties and functionalities. These materials and in particular their alloys have been long studied for thermoelectric (TE) applications around room temperature. $Bi_{2-x}Sb_xTe_3$ and $Bi_2Te_{3-x}Se_x$ are the two main p-type and n-type thermoelectric compounds respectively, used in commercial thermoelectric modules designed for room-temperature applications.[1-5] The thermoelectric module's power generation efficiency and the Peltier refrigerators' coefficient of performance are increasing function of the TE materials figure of merit, zT, where the figure of merit zT = $\sigma S^2T/\kappa$ (where σ is conductivity, S

the Seebeck coefficient, T the absolute temperature and κ the thermal conductivity). Bi_{2-x}Sb_xTe₃ compounds have shown zT values close and larger than unity.[6-11] While in general, the reported values for Bi₂Te_{3-x}Se_x are smaller, the peak value of zT is still reported to be larger than unity.[12-16]

Some of these semiconducting intermetallic compounds have been recognized as three dimensional (3D) topological insulators (TIs).[17] This new form of electronic structure in matter exhibit strong spin-orbit coupling and symmetry that contribute to generating an insulator behavior in the bulk and conducting electronic states at surfaces and interfaces.[18-20] Bi₂Se₃, in particular, has been among one of the first 3D topological insulators being identified;[17] this compound exhibits a rhombohedral phase (r-Bi₂Se₃) and a small direct bandgap of about 0.2 - 0.3 eV[17, 21-23] if grown at a relatively high temperature of the order of 200°C or above. However, growth at or below 70°C results in the crystallization to a metastable orthorhombic structure (o-Bi₂Se₃),[24] homologous to that of the compounds Bi₂S₃,[25] Sb₂S_{3,[26]} and Sb₂Se_{3[27]}. These crystal structures have larger band gaps, of the order of 0.9 - 1.2 eV, suitable for solar cells and photonic applications.[28, 29] However, the growth of a purely o-Bi₂Se₃ is difficult and rarely reported in the literature.[30-32]

in particular results Electrodeposition from nitric acidic electrolytes in a mixed-phase rhombohedral/orthorhombic variable with the relative phase fraction and the conditions of growth.[30] The conductivity of these materials is highly dependent on defect formation during growth, among which two types of Se vacancies are the dominant donor defects.[33] This results in a propensity for n-type defects, and therefore n-type conduction; the conductivity, in particular, is heavily dependent on the condition of synthesis due to the variation of defect density. Among the two phases, r-Bi₂Se₃ is widely studied for thermoelectric applications.[30, 34-40] The r-Bi₂Se₃ shows a large value of the Seebeck coefficient which makes it suitable for thermoelectric applications. The existing literature reported a Seebeck coefficient value for undoped n-type r-Bi₂Se₃ in the range of -110 μV/K to -120 μV/K.[39, 41-43] On the other hand, due to the growth issues the only reported Seebeck coefficient of the pure orthorhombic phase by Tumelero et al. shows a much higher value of -350 μV/K consistent with the large bandgap of this phase.[30]

In this work, we focus on the morphology and Seebeck coefficients of electrodeposited Bi_2Se_3 films on Au (111)/Si substrate with film thickness ranging from 0.54 μ m to 5.72 μ m. The films form continuous layers, seemingly through an anomalous Stransky-Krastanov (layer plus island) growth process, resulting in the formation of smooth films up to about 740 nm, followed by a significant roughening afterward. The Seebeck coefficient for the films exhibited a thickness-dependent variation reaching a maximum value of -

184.5 μ V/K at the 1.84 μ m film thickness. XRD patterns confirmed that the films are purely rhombohedral below 1.84 μ m thickness while film structures transition towards a mixture of orthorhombic and rhombohedral phases for the film thickness of and above 1.84 μ m. Furthermore, we theoretically calculated the Seebeck coefficients of bulk r-Bi₂Se₃ and o-Bi₂Se₃ separately from the first principle density functional theory (DFT). The experimental Seebeck coefficients match with the value of r-Bi₂Se₃ below 1.84 μ m thickness while falling between the values of pure r-Bi₂Se₃ and o-Bi₂Se₃ for 1.84 μ m and above thicknesses.

2. Experimental & Computational Details

2.1 Electrodeposition

Bi₂Se₃ films were grown onto 100 nm sputtered Au(111)/n-type Si (100) substrates. The electrolyte for electrodeposition consisted of 5 mM Bi(NO₃)₃, 5 mM SeO₂, and 0.5 M HNO₃ to increase the electrolyte conductivity and the solubility of the ionic species. The solution pH ranged from 0.2 to 0.4. The potential window to deposit Bi₂Se₃ films were between -0.1 V and -0.25 V vs. SCE. Beyond this potential, the film depoisted with an applied potential of -0.3 V appeared to have cracks on the surface. The morphology of films could deposited in this potential window exhibited variation of morphology (Fig. S1) and the Bi:Se atomic fraction for the films deposited within this potential window were found to be 38:62 (Fig. S2). However, the films deposited at -0.1 V were gray in color and appeared to be most planar and smooth from SEM images (Fig. S3). Thus, -0.1 V was chosen for potentiostatic deposition of Bi₂Se₃ on the Au/Si substrates.

The Electrodeposition experiments were carried out using the EG&G potentiostat/galvanostat by applying a constant potential of -0.1 V vs. SCE, with a front contact to the Au layer. A platinum mesh was used as the counter electrode (CE). To deposit films in a wide range of thickness, the charge density during each experiment was varied between 2 C/cm² and 13 C/cm² corresponding to 0.74 µm and 5.72 µm, respectively. The Faradaic efficiency was estimated to be around 80% by comparing the experimental thickness measured by SEM cross-sections against the thickness calculated assuming a 100% deposition efficiency. Film thickness in some cases is only indicative, due to the different morphologies of the films. The measured thickness was an average of 16 different measurements taken from two different samples grown under the same conditions.

2.2 Characterization

The stoichiometry of Bi₂Se₃ films was measured by an Energy Dispersive Spectroscopy (EDS) instrument, integrated with a Scanning Electron Microscope (SEM, FEI Quanta 650). The SEM was also used to image the morphology and microstructure of the films. The crystal structure of the films was identified with an

X-ray diffractometer (PANalytical Empyrean) with a Cu K α source (wavelength, λ = 0.154 nm), both in a Bragg-Brentano and grazing incidence modes. The average grain size of Bi₂Se₃ films was calculated using the Scherrer equation below where k, B and θ are the dimensionless shape factor, line broadening at the full width half maximum (FWHM) point of the diffraction features in the XRD pattern and the Bragg angle, respectively.

$$d = \frac{k\lambda}{BCos\theta} \tag{1}$$

Hall measurements are typically the preferred method for obtaining in-plane carrier density and mobility profiles of semiconductor thin films. Since the accuracy of carrier density profiles depends on conduction solely through the film, a non-conductive substrate is an absolute requirement for this method. Electrodeposition, on the other hand, requires the growth of thin films on a conductive substrate. Hence to perform in-plane conductivity and mobility measurements, the films need to be transferred to insulating substrates.

In this work, we focus on cross-plane electrical transport properties. An electrochemical technique, Mott-Schottky analysis, is more suitable for cross-plane carrier density analysis and was performed to obtain carrier density profiles of the Bi₂Se₃ films using a BioLogic SP-150 instrument in the frequency range of 10 Hz to 1 kHz. A 0.1 M phosphate buffer solution (PBS) was used as the electrolyte for the Mott-Schottky measurements. Carrier concentration, N_d in cm⁻³, is determined from Eq. 2, where ϵ is the permittivity of Bi₂Se₃ in F/cm, ϵ ₀ is the permittivity of free space, A is the 2-D area exposed to the electrolyte, q is the charge of an electron in C, and m is the rate of the C⁻² (cm⁴ μ F⁻²) change versus applied potential (V vs. RHE).[44]

$$N_d = \frac{2}{\varepsilon \varepsilon_o A^2 qm} \qquad (2)$$

The cross-plane electrical conductivity measurement on these samples proved to be difficult to measure. The measured values were dominated by contact resistance. To eliminate the contact resistance, usually, the transfer length measurement (TLM) is used in which resistance of samples of different thicknesses are measured and the contact resistance is extracted from the resistance versus thickness curve. However, since the mobility of the films depends on the thickness of the film (as the morphology depends on the thickness), it is not possible to separate the contact resistance using the TLM in our samples. The Seebeck coefficients were measured in the cross-plane direction using a homemade experimental setup. A 200 nm thick Au layer was deposited on the Bi₂Se₃ films as top contact for the Seebeck measurement. To obtain the Seebeck coefficient, a temperature gradient was applied to the sample along the cross-plane direction by placing the sample on top of a Peltier module. Two thermocouples and two voltage probes were used to measure the

temperature difference and the Seebeck voltage across the films respectively. The Seebeck coefficient was obtained by linearly fitting the Seebeck voltage curve with respect to the temperature difference ($S = -\Delta V/\Delta T$). All Seebeck measurements were carried out at room temperature.

2.3 Computational Details

We used density functional theory (DFT) calculation to calculate the theoretical Seebeck coefficients under constant relaxation time approximation. The Seebeck coefficient values of the rhombohedral phase and the orthorhombic phase were calculated separately. The rhombohedral unit cell of the bulk Bi₂Se₃ exhibit a space group of $R\bar{3}m$ with five atoms in the trigonal unit cell, while the orthorhombic unit cell has a space group *Pnma* with 20 atoms in the unit cell. The band structure and density of states were calculated using the plane wave DFT code, Quantum-ESPRESSO (QE),[45] treating exchange-correlation functional with generalized gradient approximation (GGA) in the form of Perdew-Burke-Ernzerhof (PBE)[46] and modified Perdew-Burke-Ernzerhof (PBEsol)[47] functional. Scalar relativistic and fully relativistic pseudopotentials are used throughout the calculation. We set the plane-wave kinetic energy cut-off at 80 Ry with a charge density of 800 Ry for both crystal structures. A 6×6×6 Monkhorst-Pack grid of k-points for the rhombohedral phase and 9×3×3 for the orthorhombic phase was used to sample the Brillouin zone.[48] The geometry relaxation calculations were performed as a result of the Born Oppenheimer approximation.[49] In this stage, the lattice parameters and the atomic coordinates were determined by minimizing the energy function within the adopted numerical approximations using the Broyden-Fletcher-Goldfarb-Shanno (BFGS) algorithm.[50] In the self-consistent calculation, the convergence threshold for energy is set to 10⁻¹⁰ eV. The band structures and density of states of the orthorhombic and rhombohedral phases are shown in Figure 6. Finally, the Seebeck coefficient calculation is done using the BoltzTrap[51] package with the semi-classical Boltzmann transport method in the constant relaxation-time[52] approximation. Within the constant relaxation-time approximation, the Seebeck coefficient can be obtained directly from the electronic structure without any adjustable parameters.

3. Results & Discussions

Fig. 1 shows the surface morphology of the Bi_2Se_3 films having thicknesses in the range of $0.74 - 5.72 \,\mu m$. Planar film deposition was observed in the early stage of growth. As the films grew in thickness, crystallized nuclei of micron-scale started to appear on the planar films. The average crystal nuclei increased with the overall film thickness; furthermore, the density of nuclei increase, and the nuclei also increased in size, forming elongated particles. The number density of these crystals presents on the surface gradually increased and at a film thickness of $^{\sim}1.84 \,\mu m$, the Bi_2Se_3 films were completely covered with crystalline

features approximately 1 μ m in length. A close-up image of one of these crystals is shown in the inset of Fig. 1.

Cross-sections for the various films are shown in Fig. 2. The films with 440 nm thickness exhibit occasional nuclei grown on the surfaces (not shown here). Around a 740 nm thickness, these nuclei transform in lamellar irregular features that result in an increase of roughness at a thickness of about 770 nm. Thicker films (1 to 5 µm) in contrast exhibit features similar to tip shapes, mostly directed in the perpendicular direction. Based on the previous SEM morphology analysis the growth mode of these films is most likely a Stransky-Krastanov mode, where the film grows initially in an epitaxial layer-by-layer, and later, beyond a critical layer thickness, which depends on the strain and the chemical potential of the deposited film, growth continues through the nucleation and coalescence of adsorbate islands. The formation of nuclei on top of the smooth Bi₂Se₃, however, occurs on a much larger scale than the usual Stransky-Krastanov, whereby few monolayers are sufficient to complete the Stransky-Krastanov growth mode. If so, we assume that the initial growth does not fully progress in an epitaxial manner, but instead follows a smooth growth where dislocations allow a quasi-epitaxial growth.

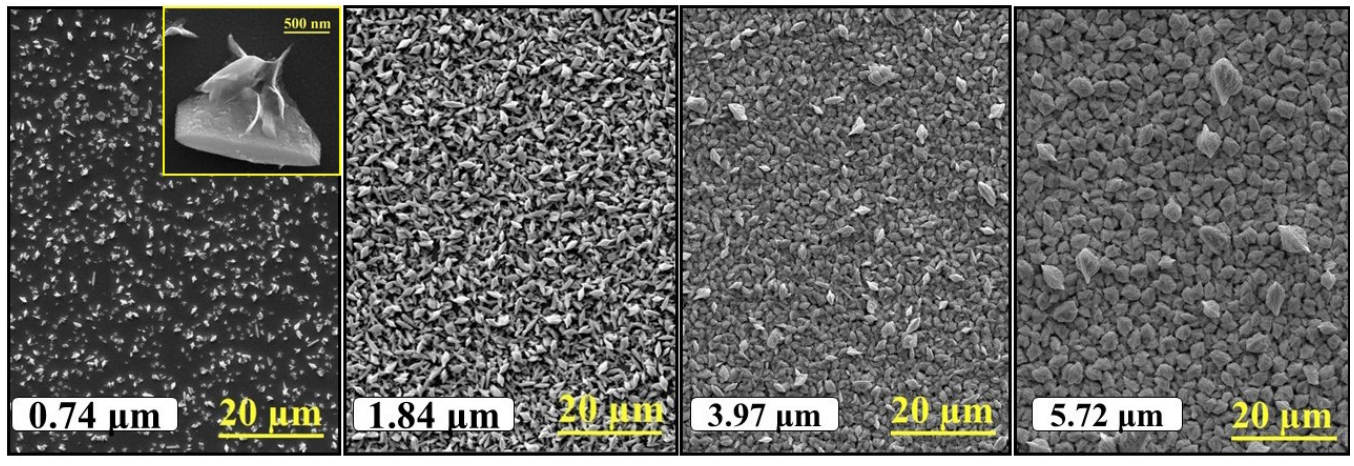


Fig. 1 Surface morphology of electrodeposited Bi₂Se₃ films with varying thicknesses.

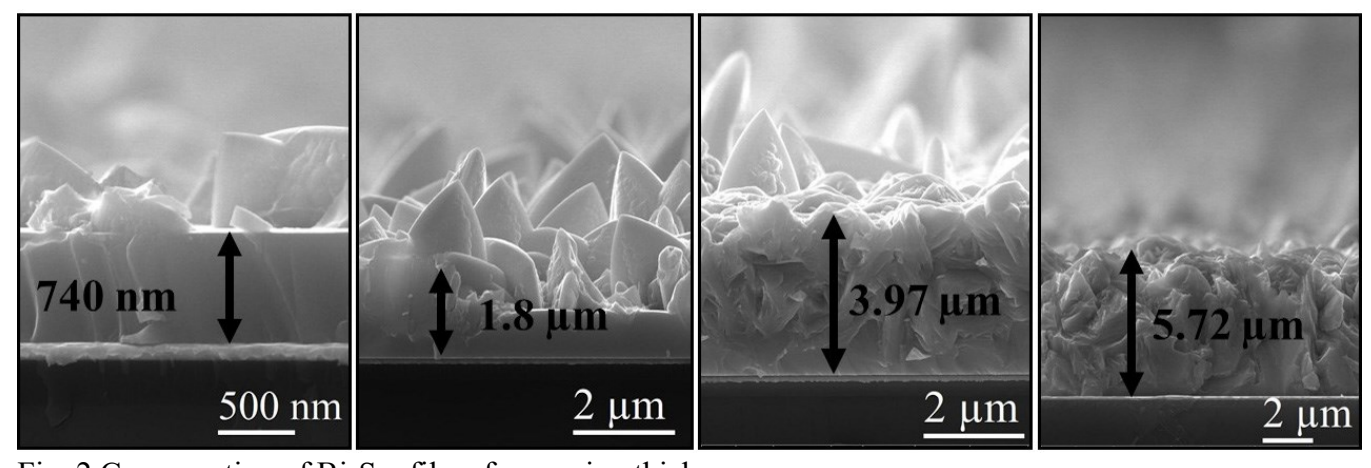


Fig. 2 Cross-section of Bi₂Se₃ films for varying thickness.

The XRD pattern of the films is shown in Fig. 3. The films corresponding to $0.74~\mu m$ thickness shows diffraction features at 2θ positions of 24.83° , 28.98° , 43.4° and 52.79° which correspond to rhombohedral (labeled as R) planes of (001), (015), (110) and (024), respectively. However, numerous new diffraction features appear in the XRD pattern of Bi₂Se₃ films having a thickness of $1.84~\mu m$, all of which corresponded to the orthorhombic (labeled O) crystal planes. The crystal structure of the Bi₂Se₃ as a function of thickness shows a dominant presence of the orthorhombic phase with respect to the rhombohedral accompanied with gradual narrowing of the reflections from the (001), (015), (110, 0111), and (024) planes suggesting the formation of larger grains in the rhombohedral phase. This is confirmed from the calculation of average grain sizes based on the Scherrer equation. The average grain size for the characteristic (015) rhombohedral plane has been included in Table 1. For further analysis, the films with thicknesses from $1.84~\mu m$ and beyond were assumed to exhibit a mixture of semiconducting orthorhombic and semi-metallic rhombohedral phases while those below $1.84~\mu m$ and less were assumed to be pure rhombohedral.

Table 1 Average film thickness, grain size, and carrier concentration in Bi₂Se₃ films

| Deposited charge | Average | Average | Carrier concentration, | |
|----------------------|-----------|------------|-----------------------------|--|
| density | thickness | grain size | N_d | |
| (C/cm ²) | (µm) | (nm) | (cm ⁻³) | |
| 2 | 0.74 | 12.9 | 1.2×10^{18} | |
| 4 | 1.84 | 25.9 | 3.04×10^{18} | |
| 9 | 3.97 | 22.2 | 5.67×10^{18} | |
| 13 | 5.72 | 30 | $1.04 \mathrm{x} \ 10^{19}$ | |

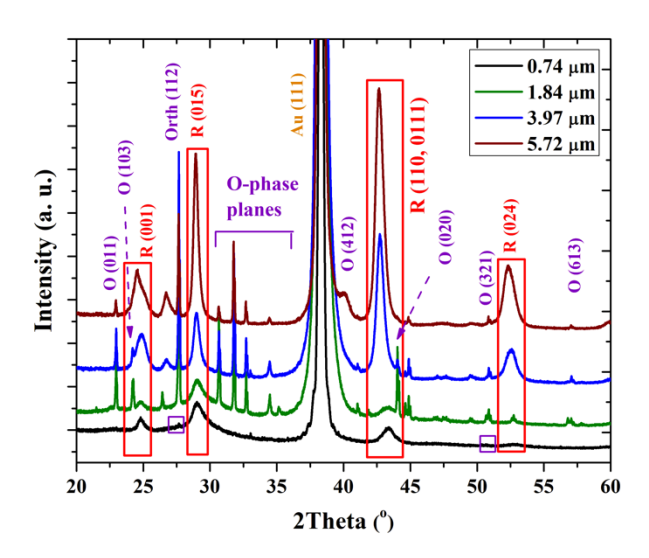


Fig. 3 XRD pattern of the Bi_2Se_3 with film thicknesses between 0.74 μm and 5.7 μm electrodeposited on Au (111) substrates.

The Mott-Schottky method was used to estimate the surface carrier concentration of the films; these data show a monotonic increase by an order of magnitude, starting from $1.2 \times 10^{18} \, \text{cm}^{-3}$ for a $0.74 \, \mu \text{m}$ thick film, up to $1.04 \times 10^{19} \, \text{cm}^{-3}$ for $5.72 \, \mu \text{m}$ films. The $1/C^2$ vs. potential plot used to determine the carrier concentration for the films are shown in Fig. 4, and N_d values are included in Table 1. The positive slope of the Mott-Schottky plots confirms the n-type conductivity of the films (Fig. 4), as validated from the negative Seebeck coefficients. This is consistent with Se-rich films. The atomic ratio of Bi:Se in these electrodeposited films were 38:62. Under such Se-rich conditions, Se-antisites (Se_{Bi}) show the lowest formation energy and therefore the most likely point defect, leading to n-type conductivity in rhombohedral Bi₂Se₃.[33] In the case of the pure orthorhombic phase, Se antisites (Se_{Bi}) are more likely owing to lower formation energies in Se-rich films, thus leading to n-type conductivity.[53]

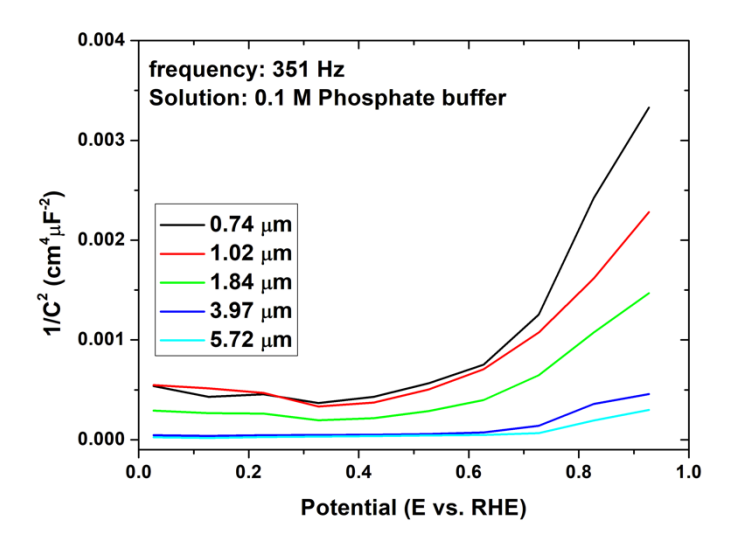


Fig. 4 Mott-Schottky plots of the Bi_2Se_3 with film thicknesses between 0.74 μm and 5.72 μm electrodeposited on Au (111) substrates.

The variation of experimentally measured room temperature Seebeck coefficients (S) as a function of Bi₂Se₃ film thickness is shown in Fig. 5. The negative sign of the Seebeck values indicates n-type conduction in the films. The room temperature Seebeck coefficient for 0.74 μ m thick films was around - 90.5 μ V/K which gradually increased to a maximum of -184.5 μ V/K when the film thickness reached 1.84 μ m. The Seebeck coefficient of the films decreases beyond this thickness value to -100.8 μ V/K for a film thickness of 5.72 μ m.

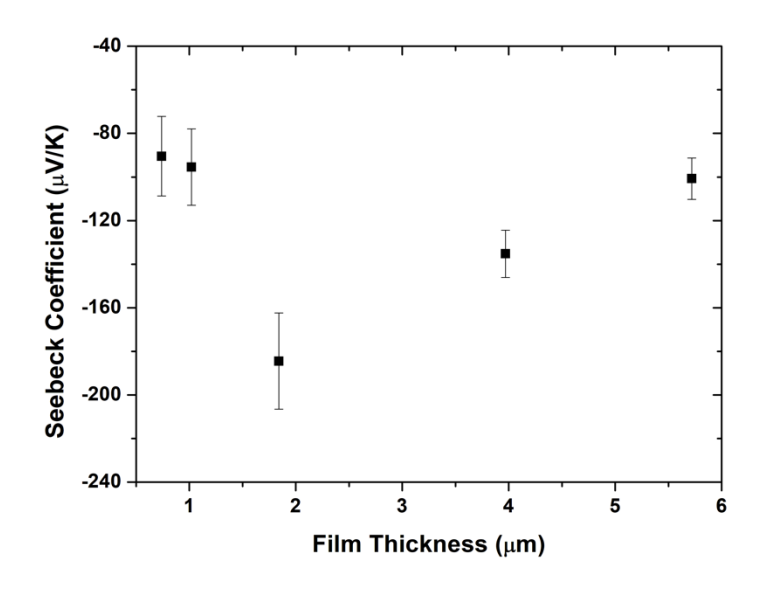


Fig. 5 Experimentally determined Seebeck coefficients of the Bi_2Se_3 films with film thickness between 0.74 μm to 5.72 μm .

Previous reports on experimental Seebeck coefficients of Bi_2Se_3 are summarized in Table 2. A majority of the existing literature reports Seebeck coefficients between -100 μ V/K and -120 μ V/K for n-type conductivity. The increase of surface roughness in the morphology of the films due to crystal formations in the 0.74 – 1.84 μ m film range were also taken into consideration to explain the increasing Seebeck coefficient trend. The presence of porosity in the film morphology may result in enhanced scattering of low energy carriers with higher efficiency compared to planar structures; this results in an enhanced Seebeck effect.[54] The only reported Seebeck coefficient of the pure orthorhombic phase shows a much higher value of -350 μ V/K which is significantly higher than those observed for the rhombohedral phase.[30] Thus, the emergence of a dominant orthorhombic phase in our films (higher in phase fraction) around 1.84 μ m thickness was most likely the factor that contributed to the improvement of the Seebeck coefficient.

To further explain the variation of Seebeck coefficients, we theoretically calculated the Seebeck coefficients. In theory, it is not feasible to calculate the Seebeck coefficients of mixed-phase Bi₂Se₃ using first-principles calculations. Instead, the Seebeck coefficients of bulk r-Bi₂Se₃ and o-Bi₂Se₃ are calculated separately. The films are thick enough to be considered as bulk. Since the exact volume fractions are not known, we can only determine the range of the Seebeck coefficient variations. The differential conductivity $\sigma(E)$, the conductivity σ , and the Seebeck coefficient S are given respectively by Eq. 3 – 5.

$$\sigma(E) = q^{2}g(E)v^{2}(E)\tau(E) - - - (3)$$

$$\sigma = \int \sigma(E) \left(-\frac{\partial f}{\partial \varepsilon}\right) dE - - - (4)$$

$$S = -\frac{1}{qT} \frac{\int \sigma(E) (E - \mu) \left(-\frac{\partial f}{\partial E}\right) dE}{\int \sigma(E) \left(-\frac{\partial f}{\partial E}\right) dE} - - - (5)$$

Where E is the energy, g(E) is the density of states, q is the electronic charge, v(E) is the group velocity, $\tau(E)$ is the relaxation time, f is the Fermi-Dirac distribution function, μ is the chemical potential and T is the temperature. For metals and degenerate semiconductors, the Seebeck coefficient can be approximated by the Mott formula.^[55]

$$S = \frac{\pi^2}{3} \left(\frac{\kappa_B^2 T}{e} \right) \left(\frac{d \log \sigma(E)}{dE} \right)_{E=\mu} - - - (6)$$

Table 2 Reported Seebeck coefficients of Bi₂Se₃

| Deposition Metho | d | Film type | Crystal | Seebeck |
|-------------------------|----------|--------------------------|----------------|-------------|
| | | | Structure | Coefficient |
| | | | | $(\mu V/K)$ |
| Solvothermal[39] | | Nanostructures | R* | -115 |
| Electrodeposition[36] | | Films | R | +26.46 |
| | | | M^* | +6.53 |
| Aqueous | Chemical | Nanostructured films | R | -119 |
| Growth[56] | | | | |
| Electrodeposition[30] | | Films | O^* | -350 |
| MOCVD[41] | | Films | R | -120 |
| MBE[43] | | 30 quintuple layers (QL) | - | -104.3 |
| Aqueous | Chemical | Nanostructured films | R | -113 |
| growth[42] | | | | |
| Electrodeposition[57] | | Films | R | +20 |

^{*}The rhombohedral, mixed-phase and orthorhombic crystal structures are denoted as R, M, and O

Thus, the electronic band structure and density of states of material play a key role in determining the thermoelectric properties of the system in question. The r-Bi₂Se₃ and the o-Bi₂Se₃ have completely different electronic band structures and density of states as shown in Fig. 6. The r-Bi₂Se₃ shows a narrow bandgap of 0.24 eV while the o-Bi₂Se₃ shows a wide bandgap of around 0.95 eV. The calculated bandgaps of r-Bi₂Se₃ and o-Bi₂Se₃ are consistent with previous theoretical and experimental bandgaps of 0.2 - 0.3 eV[17, 21-23], and 0.9 - 1.2 eV[28, 29], respectively.

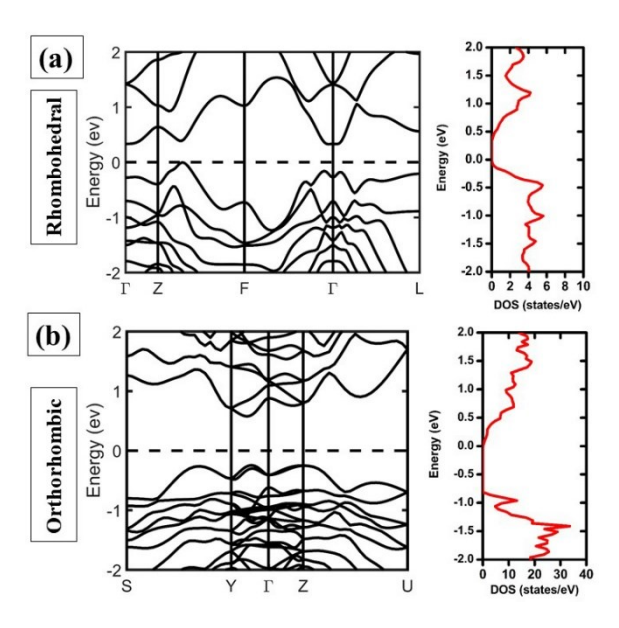


Fig. 6 Theoretical band structure and density of states of (a) rhombohedral phase Bi₂Se₃ and (b) orthorhombic phase Bi₂Se₃.

The Seebeck coefficient depends mainly on the position of the Fermi level (carrier concentration) and the energy dependence of the density of state and the relaxation times. Owing to their different electronic structure, the r-Bi₂Se₃ and o-Bi₂Se₃ give rise to a different range of Seebeck coefficients which are plotted as a function of carrier concentration in Fig. 7a. The Seebeck coefficients of r-Bi₂Se₃ and o-Bi₂Se₃ are extracted for each film using the carrier concentration values that are obtained from the Mott-Schottky analysis. The theoretical Seebeck coefficients of the pure r-Bi₂Se₃ and o-Bi₂Se₃ are shown in Fig. 7b along with our experimental Seebeck coefficients of the mixed phases. Our observed experimental values match those for the pure rhombohedral phase in the $0.74 - 1.02 \,\mu m$ thickness range. However, for films with 1.84 $\,\mu m$ thickness, the experimental Seebeck coefficient matches that for the pure orthorhombic phase more closely. For thicker films (3.97 $\,\mu m$ and 5.72 $\,\mu m$) the experimental values were within the limits set by the theory for pure r-Bi₂Se₃ and o-Bi₂Se₃. These results agree with our conclusions of the mixed-phase structure of films based on the analysis of XRD patterns.

The increasing trend of carrier concentration with film thickness (Fig. 5d) would generally lead to decreasing Seebeck coefficient values. However, in our study, we observe that this trend holds only in the $1.84-5.72~\mu m$ thickness range, where a mixture of rhombohedral and orthorhombic phases co-exists. On the other hand, the increasing Seebeck coefficient trend is observed in the $0.74-1.84~\mu m$ thickness range, where the onset of crystal formation and growth of the orthorhombic phase in the films occurred. The phase

fraction of the films could not be estimated with a reasonable degree of certainty by analyzing data from XRD pattern and Raman spectroscopy, which limited our ability to match the observed values to the predicted Seebeck coefficient values with higher accuracy.

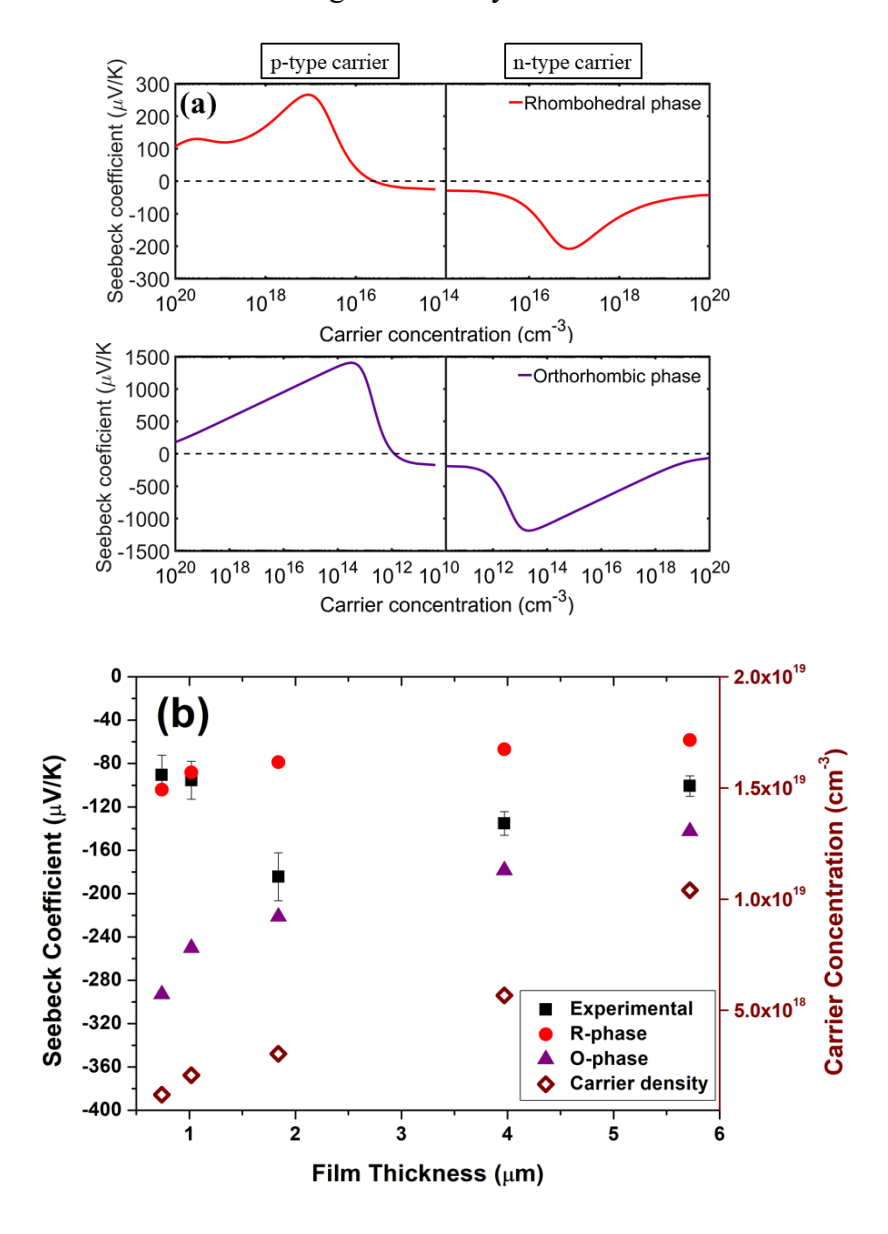


Fig. 7 (a) Theoretically calculated Seebeck coefficient vs. carrier or doping density plots and (b) comparison of experimental measurements of mixed-phase Bi₂Se₃ films (black squares) and theoretical Seebeck coefficients of pure rhombohedral (red circles) and pure orthorhombic (purple triangles) phases of Bi₂Se₃ films.

5 Conclusions

The electrodeposited Bi₂Se₃ films upon nucleation form continuous layers following the Stransky-Krastanov (layer plus island) growth process and resulting in the formation of smooth films up to about

700 nm thickness. In later stages film growth is dominated by the formation of crystals which coalesce together to form a rougher film. XRD patterns confirmed that the films are purely r-Bi₂Se₃ below 1.84 μ m thickness while they are mixed-phase Bi₂Se₃ for 1.84 μ m thickness and beyond. The Seebeck coefficient shows n-type conductivity, exhibiting a maximum value of -184 μ V/K at 1.84 μ m thickness. First-principles calculations were implemented to calculate the band structure of the rhombohedral and orthorhombic phases and the obtained bandgaps closely replicate those of the experiment. The Seebeck coefficient values were calculated using constant relaxation times. From the theoretically obtained Seebeck coefficients, it is shown that the experimental Seebeck coefficients match the values of the rhombohedral phase when the film thickness is below 1.84 μ m while falling between the Seebeck coefficients of pure rhombohedral and orthorhombic phase when the film thickness is 1.84 μ m and above.

Conflicts of interest

There are no conflicts to declare.

Acknowledgments

MG Rosul and M Zebarjadi would like to acknowledge the funding support from the National Science Foundation grant number 1653268. R Ahmed, Y Xu and G Zangari would like to acknowledge the financial support from the University of Virginia through the MAXNET Energy Partnership.

References

- [1] Z. Ren, Y. Lan, Q. Zhang, Advanced thermoelectrics: materials, contacts, devices, and systems, CRC Press2017.
- [2] H.J. Goldsmid, Introduction to thermoelectricity, Springer2010.
- [3] J. Schilz, L. Helmers, W. Müller, M. Niino, A local selection criterion for the composition of graded thermoelectric generators, Journal of applied physics, 83 (1998) 1150-1152.
- [4] A.F. Ioffe, Semiconductor thermoelements and thermoelectric cooling, (1957).
- [5] M.-K. Kim, M.-S. Kim, S. Lee, C. Kim, Y.-J. Kim, Wearable thermoelectric generator for harvesting human body heat energy, Smart Materials and Structures, 23 (2014) 105002.
- [6] S.I. Kim, K.H. Lee, H.A. Mun, H.S. Kim, S.W. Hwang, J.W. Roh, D.J. Yang, W.H. Shin, X.S. Li, Y.H. Lee, Dense dislocation arrays embedded in grain boundaries for high-performance bulk thermoelectrics, Science, 348 (2015) 109-114.
- [7] S. Gao, J. Gaskins, X. Hu, K. Tomko, P. Hopkins, S.J. Poon, enhanced figure of Merit in Bismuth-Antimony fine-Grained Alloys at cryogenic temperatures, Scientific reports, 9 (2019) 1-10.
- [8] B. Poudel, Q. Hao, Y. Ma, Y. Lan, A. Minnich, B. Yu, X. Yan, D. Wang, A. Muto, D. Vashaee, High-thermoelectric performance of nanostructured bismuth antimony telluride bulk alloys, Science, 320 (2008) 634-638.
- [9] M. Rull-Bravo, A. Moure, J. Fernandez, M. Martín-González, Skutterudites as thermoelectric materials: revisited, Rsc Advances, 5 (2015) 41653-41667.
- [10] A.M. Dehkordi, M. Zebarjadi, J. He, T.M. Tritt, Thermoelectric power factor: Enhancement mechanisms and strategies for higher performance thermoelectric materials, Materials Science and Engineering: R: Reports, 97 (2015) 1-22.
- [11] G. Smith, R. Wolfe, Thermoelectric Properties of Bismuth-Antimony Alloys, Journal of Applied Physics, 33 (1962) 841-846.

- [12] S. Wang, W. Xie, H. Li, X. Tang, Enhanced performances of melt spun Bi2 (Te, Se) 3 for n-type thermoelectric legs, Intermetallics, 19 (2011) 1024-1031.
- [13] S. Wang, G. Tan, W. Xie, G. Zheng, H. Li, J. Yang, X. Tang, Enhanced thermoelectric properties of Bi 2 (Te 1– x Se x) 3-based compounds as n-type legs for low-temperature power generation, Journal of Materials Chemistry, 22 (2012) 20943-20951.
- [14] O. Yamashita, S. Tomiyoshi, High performance n-type bismuth telluride with highly stable thermoelectric figure of merit, Journal of Applied Physics, 95 (2004) 6277-6283.
- [15] S. Wang, H. Li, R. Lu, G. Zheng, X. Tang, Metal nanoparticle decorated n-type Bi2Te3-based materials with enhanced thermoelectric performances, Nanotechnology, 24 (2013) 285702.
- [16] I.T. Witting, F. Ricci, T.C. Chasapis, G. Hautier, G.J. Snyder, The Thermoelectric Properties of -Type Bismuth Telluride: Bismuth Selenide Alloys, Research, 2020 (2020) 15.
- [17] H. Zhang, C.-X. Liu, X.-L. Qi, X. Dai, Z. Fang, S.-C. Zhang, Topological insulators in Bi2Se3, Bi2Te3 and Sb2Te3 with a single Dirac cone on the surface, Nature Physics, 5 (2009) 438-442.
- [18] S. Singh, K. Kaur, R. Kumar, Quest of thermoelectricity in topological insulators: A density functional theory study, Applied Surface Science, 418 (2017) 232-237.
- [19] K. Pal, S. Anand, U.V. Waghmare, Thermoelectric properties of materials with nontrivial electronic topology, Journal of Materials Chemistry C, 3 (2015) 12130-12139.
- [20] H. Osterhage, J. Gooth, B. Hamdou, P. Gwozdz, R. Zierold, K. Nielsch, Thermoelectric properties of topological insulator Bi2Te3, Sb2Te3, and Bi2Se3 thin film quantum wells, Applied Physics Letters, 105 (2014) 123117.
- [21] J. Black, E. Conwell, L. Seigle, C. Spencer, Electrical and optical properties of some M2v-bN3vi-b semiconductors, Journal of Physics and Chemistry of Solids, 2 (1957) 240-251.
- [22] S. Mishra, S. Satpathy, O. Jepsen, Electronic structure and thermoelectric properties of bismuth telluride and bismuth selenide, Journal of Physics: Condensed Matter, 9 (1997) 461.
- [23] E. Mooser, W. Pearson, New semiconducting compounds, Physical Review, 101 (1956) 492.
- [24] R. Ahmed, Q. Lin, Y. Xu, G. Zangari, Growth, morphology and crystal structure of electrodeposited Bi2Se3 films: Influence of the substrate, Electrochimica Acta, 299 (2019) 654-662.
- [25] H. Moreno-Garcia, M.T.S. Nair, P.K. Nair, All-chemically deposited Bi2S3/PbS solar cells, Thin Solid Films, 519 (2011) 7364-7368.
- [26] D.-H. Kim, S.-J. Lee, M. Park, J.-K. Kang, J. Heo, S. Im, S.-J. Sung, Highly reproducible planar Sb2S3-sensitized solar cells based on atomic layer deposition, Nanoscale, 6 (2014) 14549-14554.
- [27] Y. Zhou, L. Wang, S. Chen, S. Qin, X. Liu, J. Chen, D.-J. Xue, M. Luo, Y. Cao, Y. Cheng, E. Sargent, J. Tang, Thin-film Sb2Se3 photovoltaics with oriented one-dimensional ribbons and benign grain boundaries, Nature Photonics, 9 (2015) 409-415.
- [28] M. Tumelero, L. Benetti, E. Isoppo, R. Faccio, G. Zangari, A. Pasa, Electrodeposition and ab Initio Studies of Metastable Orthorhombic Bi2Se3: A Novel Semiconductor with Bandgap for Photovoltaic Applications, Journal of Physical Chemistry C, 120 (2016) 11797-11806.
- [29] M. Filip, C. Patrick, F. Giustino, G W quasiparticle band structures of stibnite, antimonselite, bismuthinite, and guanajuatite, 87 (2013).
- [30] M.A. Tumelero, M.B. Martins, P.B. Souza, R.D. Della Pace, A.A. Pasa, Effect of electrolyte on the growth of thermoelectric Bi2Se3 thin films, Electrochimica Acta, 300 (2019) 357-362.
- [31] C. Xiao, J. Yang, W. Zhu, J. Peng, J. Zhang, Electrodeposition and characterization of Bi2Se3 thin films by electrochemical atomic layer epitaxy (ECALE), Electrochimica Acta, 54 (2009) 6821-6826.
- [32] N. Patil, A. Sargar, S. Mane, P. Bhosale, Growth mechanism and characterisation of chemically grown Sb doped Bi2Se3 thin films, Applied Surface Science, 254 (2008) 5261-5265.
- [33] D.O. Scanlon, P.D.C. King, R.P. Singh, A. de la Torre, M. Walker, G. Balakrishnan, F. Baumberger, C.R.A. Catlow, Controlling Bulk Conductivity in Topological Insulators: Key Role of Anti-Site Defects, Advanced Materials, 24 (2012) 2154-2158.
- [34] Y. Sun, H. Cheng, S. Gao, Q. Liu, Z. Sun, C. Xiao, C. Wu, S. Wei, Y. Xie, Atomically thick bismuth selenide freestanding single layers achieving enhanced thermoelectric energy harvesting, Journal of the American Chemical Society, 134 (2012) 20294-20297.
- [35] Y.S. Hor, P. Roushan, H. Beidenkopf, J. Seo, D. Qu, J.G. Checkelsky, L.A. Wray, D. Hsieh, Y. Xia, S.-Y. Xu, Development of ferromagnetism in the doped topological insulator Bi 2– x Mn x Te 3, Physical Review B, 81 (2010) 195203.

- [36] X.-l. Li, K.-f. Cai, H. Li, L. Wang, C.-w. Zhou, Electrodeposition and characterization of thermoelectric Bi2Se3 thin films, International Journal of Minerals, Metallurgy, and Materials, 17 (2010) 104-107.
- [37] C. Kulsi, K. Kargupta, S. Ganguly, D. Banerjee, Enhanced thermoelectric performance of n-type bismuth selenide doped with nickel, Current Applied Physics, 17 (2017) 1609-1615.
- [38] Y. Min, J.W. Roh, H. Yang, M. Park, S.I. Kim, S. Hwang, S.M. Lee, K.H. Lee, U. Jeong, Surfactant-Free Scalable Synthesis of Bi2Te3 and Bi2Se3 Nanoflakes and Enhanced Thermoelectric Properties of Their Nanocomposites, Advanced Materials, 25 (2013) 1425-1429.
- [39] K. Kadel, L. Kumari, W.Z. Li, J. Huang, P. Provencio, Synthesis and Thermoelectric Properties of Bi2Se3 Nanostructures, Nanoscale Research Letters, 6 (2010).
- [40] Z. Ali, S. Butt, C. Cao, F.K. Butt, M. Tahir, M. Tanveer, Í. Aslam, M. Rizwan, F. Idrees, S. Khalid, Thermochemically evolved nanoplatelets of bismuth selenide with enhanced thermoelectric figure of merit, AIP Advances, 4 (2014) 117129.
- [41] A. Al Bayaz, A. Giani, M. Al Khalfioui, A. Foucaran, F. Pascal-Delannoy, A. Boyer, Growth parameters effect on the thermoelectric characteristics of Bi2Se3 thin films grown by MOCVD system using Ditertiarybutylselenide as a precursor, Journal of crystal growth, 258 (2003) 135-140. [42] Z. Sun, S. Liufu, L. Chen, Synthesis and characterization of nanostructured bismuth selenide thin films, Dalton Transactions, 39 (2010) 10883.
- [43] M. Guo, Z. Wang, Y. Xu, H. Huang, Y. Zang, C. Liu, W. Duan, Z. Gan, S.-C. Zhang, K. He, Tuning thermoelectricity in a Bi2Se3 topological insulator via varied film thickness, New Journal of Physics, 18 (2016) 015008.
- [44] K. Gelderman, L. Lee, S.W. Donne, Flat-Band Potential of a Semiconductor: Using the Mott–Schottky Equation, J. Chem. Educ., 84 (2007) 685.
- [45] P. Giannozzi, S. Baroni, N. Bonini, M. Calandra, R. Car, C. Cavazzoni, D. Ceresoli, G.L. Chiarotti, M. Cococcioni, I. Dabo, QUANTUM ESPRESSO: a modular and open-source software project for quantum simulations of materials, Journal of physics: Condensed matter, 21 (2009) 395502.
- [46] J.P. Perdew, K. Burke, M. Ernzerhof, Generalized gradient approximation made simple, Physical review letters, 77 (1996) 3865.
- [47] J.P. Perdew, A. Ruzsinszky, G.I. Csonka, O.A. Vydrov, G.E. Scuseria, L.A. Constantin, X. Zhou, K. Burke, Restoring the density-gradient expansion for exchange in solids and surfaces, Physical review letters, 100 (2008) 136406.
- [48] H.J. Monkhorst, J.D. Pack, Special points for Brillouin-zone integrations, Physical review B, 13 (1976) 5188.
- [49] M. Born, R. Oppenheimer, Zur quantentheorie der molekeln, Annalen der physik, 389 (1927) 457-484.
- [50] R. Fletcher, Practical methods of optimization, John Wiley & Sons2013.
- [51] G.K. Madsen, D.J. Singh, BoltzTraP. A code for calculating band-structure dependent quantities, Computer Physics Communications, 175 (2006) 67-71.
- [52] B.R. Nag, Electron transport in compound semiconductors, Springer Science & Business Media2012.
- [53] M. Tumelero, R. Faccio, A. Pasa, The role of interstitial native defects in the topological insulator Bi2Se3, Journal of Physics: Condensed Matter, 28 (2016).
- [54] K. Valalaki, P. Benech, A.G. Nassiopoulou, High Seebeck coefficient of porous silicon: study of the porosity dependence, Nanoscale research letters, 11 (2016) 201.
- [55] M. Jonson, G. Mahan, Mott's formula for the thermopower and the Wiedemann-Franz law, Physical Review B, 21 (1980) 4223.
- [56] X. Qiu, L.N. Austin, P.A. Muscarella, J.S. Dyck, C. Burda, Nanostructured Bi2Se3 films and their thermoelectric transport properties, Angewandte Chemie International Edition, 45 (2006) 5656-5659.
- [57] L. Xiaolong, X. Zhen, The effect of electrochemical conditions on morphology and properties of Bi2Se3 thick films by electrodeposition, Materials Letters, 129 (2014) 1-4.